

# Towards Semantic 3D Hand-Object Interaction Generation via Functional Text Guidance

Yongqi Tian\*    Xueyu Sun\*    Haoyuan He    Linji Hao    Ning Ding    Caigui Jiang<sup>†</sup>

Xi'an Jiaotong University

{yongqitian, xueyusun, hehy02, 897247280}@stu.xjtu.edu.cn

yuji.dn@alibaba-inc.com

cgjiang@xjtu.edu.cn

## Abstract

*Hand-object interaction (HOI) is the fundamental link between human and environment, yet its dexterous and complex pose significantly challenges for gesture control. Despite significant advances in AI and robotics, enabling machines to understand and simulate hand-object interactions, capturing the semantics of functional grasping tasks remains a considerable challenge. While previous work can generate stable and correct 3D grasps, they are still far from achieving functional grasps due to unconsidered grasp semantics. To address this challenge, we propose an innovative two-stage framework, Functional Grasp Synthesis Net (FGS-Net), for generating 3D HOI driven by functional text. This framework consists of a text-guided 3D model generator, Functional Grasp Generator (FGG), and a pose optimization strategy, Functional Grasp Refiner (FGR). FGG generates 3D models of hands and objects based on text input, while FGR fine-tunes the poses using Object Pose Approximator and energy functions to ensure the relative position between the hand and object aligns with human intent and remains physically plausible. Extensive experiments demonstrate that our approach achieves precise and high-quality HOI generation without requiring additional 3D annotation data.*

## 1. Introduction

The hand plays a crucial role in interacting with objects in the surrounding world, performing tasks ranging from 'drink water' to 'take a photo'. Humans continuously interact with objects through their hands to perform a variety of daily activities, such as eating and working. In recent years, an increasing number of HOI datasets [6, 9–11, 20, 38] have been created to facilitate machine learning research on human grasping behaviors [12, 15, 40]. However, these efforts

have ignored the importance of aligning grasps with human intent, focusing instead on stable grasping. The conducting of complex interaction tasks relies not only on the shapes of objects but also on human intent. Existing methods for HOI have established a relationship with textual descriptions [1, 21, 30, 32]; however, they have yet to address the human intent behind functional grasp, such as 'drink water' or 'read a book', which involves higher-level semantics. This task requires machines to generate appropriate grasps based on the geometries of different objects, while also enabling more controllable interaction via functional text prompts. Enabling machines to comprehend and control HOI guided by functional tasks is still a significant challenge.

Previous methods [1, 30, 42] have already established the relationship between text and grasping. However, these methods face inherent ambiguities when dealing with functional text-driven grasping, primarily in two aspects: 1. '**How to grasp**', which is typically linked to the task description text and the object characteristics that align with it closely, relies on the task description to provide the contextual information necessary for grasping, while the object characteristics provide the basis for generating the hand shape; 2. '**Where to grasp**', which is tightly related to the task description text and the geometric shape of the object, depends not only on the implied intentions in the text but also on the geometric characteristics of the object to ensure the accuracy and effectiveness of the grasp position.

In addition, obtaining relevant data remains a significant challenge in this field, as high-quality 3D annotated data and detailed interaction videos are typically difficult to obtain, limiting the scalability and generalization capabilities of models. Some studies [4, 5, 14, 45] attempted to train models to understand object interactions using publicly available 3D annotated data. However, these datasets often require complex motion capture devices and substantial resource investment. Previous methods [7, 12, 42] managed to achieve high-quality 3D HOI reconstruction using

\*Equal contribution.

<sup>†</sup>Corresponding author

video data; however, high-quality videos equipped with detailed interaction annotations are still rare. Therefore, learning HOI without relying on additional 3D annotations and video data is a promising research direction. Fig. ?? illustrates our results: six 3D HOI syntheses generated via functional text, displayed from four different perspectives.

In this work, we propose a human-object interaction generation framework, Functional Grasp Synthesis Net (FGS-Net), driven by functional text to create corresponding 3D HOI models. Our approach follows a two-stage method, comprising a text-guided 3D hand and object generation model Functional Grasp Generator and a pose refining strategy Functional Grasp Refiner. FGG takes text input to generate the corresponding 3D models of the hand and object, while FGR refines the relative posture between the hand and object using Object Pose Approximator and contact optimization.

In summary, our contributions are as follows:

- We propose **FGS-Net**, which extends 3D HOI generation using functional text prompts, enabling grasp control that more closely aligns with human intentions.
- We introduce a two-stage method comprising a functional text-guided hand-object model generation module, **FGG**, and a pose optimization module, **FGR**. Given a text prompt, **FGG** generates 3D models of the hand and object, followed by the application of **FGR** to ensure the plausibility of the grasp.
- Extensive experiments demonstrate that our method achieves state-of-the-art performance compared to other reconstruction and grasp synthesis methods that align with human intentions, without requiring additional 3D annotations.

## 2. Related Works

**3D HOI Reconstruction:** This task aims to reconstruct the 3D geometry of hands and the objects they hold from images [4, 5, 12, 14, 42]. Existing methods are generally categorized into two types: multi-view reconstruction and single-view reconstruction. Multi-view reconstruction methods [2, 9, 22, 39] typically employ multiple cameras positioned at various viewpoints to infer the 3D structure of the grasping scenario. Although this type of method can produce highly accurate 3D reconstruction results, they require precise camera calibration and are not easily deployable in outdoor scenes. On the other hand, single-view methods are inherently ill-posed. Therefore, using parametric models such as MANO [26] can alleviate the hand reconstruction problem. These models provide low-dimensional representations of hands, facilitating the mapping to detailed mesh models. Building on this foundation, deep learning methods use visual network models as the backbone and introduce downstream task heads within the architecture to predict the hand parameters of the parametric

models, thereby completing the 3D reconstruction [23, 27].

**Physical HOI Synthesis** Several studies on the synthesis of HOI have focused on integrating physical and spatial guidance to ensure the production of physically plausible scenarios [8, 19, 33, 34, 37]. These approaches optimize the physical interactions between hands and objects, aiming to generate 3D HOI data that adheres to established physical laws for enhanced realism. Inspired by these efforts, our work further refines the synthesis process by introducing a set of combined loss terms specifically designed to enhance the reality of 3D HOI.

**Task-Oriented HOI Synthesis** Task-oriented HOI synthesis aims to model the connection between abstract high-level task semantics and dexterous hand-object interactions, targeting different tasks for the same category of objects. Recent works combine 3D segmentation frameworks to provide more fine-grained task-semantic-related optimization objectives, synthesizing HOI scenes for different high-level abstract tasks [1, 3, 35, 36, 47]. However, these methods intuitively introduce additional data annotation, which results in a labor-intensive workload. Our method, while being 3D label-free, extends HOI synthesis to generate task-oriented hand-object interactions starting from different abstract task descriptions.

Overall, without the need for carefully selected additional 3D annotations, we propose a system capable of accomplishing task-oriented HOI synthesis based on various task prompts.

## 3. Method

Given a functional text, our framework aims to generate the corresponding hand-object interaction 3D model. Overall, we propose a two-stage method, Functional Grasp Synthesis Net (FGS-Net): first, Functional Grasp Generator (FGG) generates functional grasp and the corresponding 3D model of the object. Next, Functional Grasp Refiner (FGR) is utilized to refine the hand-object pose. An overview can be seen in Fig. 1.

The subsequent sections are organized as follows: first, we clarify our use of diffusion models to learn interaction priors in Section 3.1. The FGG method will be detailed in Section 3.2. Finally, in Section 3.3, we provide an in-depth explanation of the FGR refining process for HOI we developed.

### 3.1. Leveraging Data to Learn Interactive Priors

Considering the challenges in acquiring 3D prior information for HOI due to the complexity of interaction scenarios, differences in perspectives, and the high cost of data annotation, this study adopts a Diffusion model [25] to learn the joint probability distribution of HOI and the objects themselves, aiming to construct a geometric prior for functional interactions.

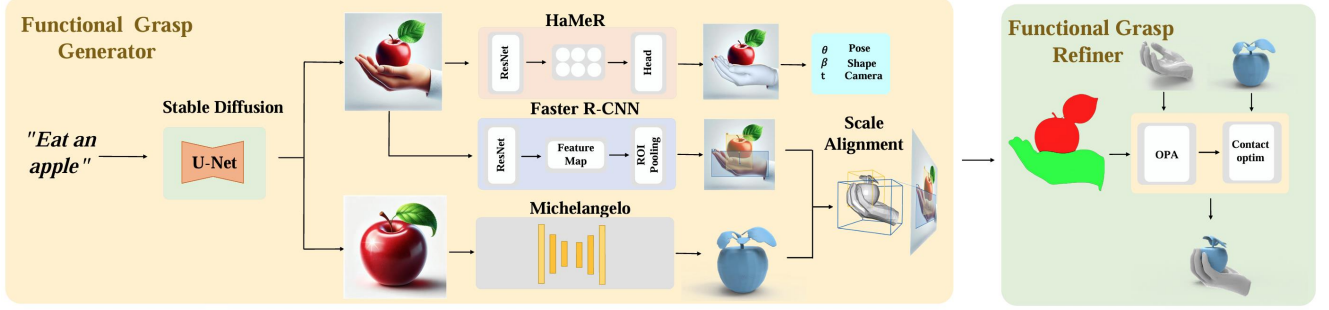


Figure 1. **The overview of our work:** We propose a two-stage method for generating 3D models of hand-object interactions. Given a task prompt, FGG generates a hand and object that conform to the prompt, while simultaneously estimating the hand pose and aligning the sizes of the hand and object. Subsequently, FGR is applied to refine the position of the HOI, including an Object Pose Approximator and an energy function guided hand-object contact optimization.

**Interactive Priors for Diffusion Models:** Denoising Diffusion Probabilistic Models (DDPMs) [13] are latent variable based models inspired by non-equilibrium thermodynamics for high-quality image synthesis. DDPM works by training a parameterized Markov chain that reverses a diffusion process that gradually adds noise to the data over a finite amount of time, thereby generating samples that match the data distribution. The core idea is:

$$p_{\theta}(x_0 : T) := p(x_T) \prod_{t=1}^T p_{\theta}(x_{t-1} | x_t) \quad (1)$$

Among these,  $p(x_T)$  is the prior distribution, typically a Gaussian noise distribution, while  $p_{\theta}(x_{t-1} | x_t)$  represents the conditional Gaussian transition probability at each time step  $t$  which denotes the recovery from the noisy data  $x_t$  to  $x_{t-1}$ .

**Tuning Diffusion Parameters:** Functional text is incorporated as external conditional information into the diffusion model to jointly denoise images depicting interactions between objects and hands. In this framework, the functional text  $T$  is embedded using a CLIP [24] encoder and fine-tuning of the diffusion model is performed via the DreamBooth [28]. The training data consists of both HOI

images  $I_{\text{hoi}}$  and object images  $I_{\text{obj}}$ . The objective of the diffusion model  $G$  is to generate HOI and object images that align with the textual description, guided by the functional text  $T$ :

$$I_{\text{hoi}}, I_{\text{obj}} = G(T) \quad (2)$$

Meanwhile, we employ a conditional diffusion model pre-trained on a large-scale dataset of text-image pairs [25].

### 3.2. Functional 3D HOI Elements Initialization

**Hand Representation and Reconstruction:** We use MANO [11, 26] as the hand representation for 3D HOI scenarios. MANO is a parametric model which provides a template mesh model of a standard hand  $\mathcal{M}_{\text{std}}$ , and models various appearances and poses of the hand using low-dimensional shape parameters  $\beta$  and pose parameters  $\theta$ , allowing for the generation of corresponding hand mesh models  $\mathcal{M}_h = \text{MANO}(\theta, \beta; \mathcal{M}_{\text{std}})$ .

Optimizing HOI in 2D is challenging while validating its effectiveness is difficult. To obtain more refined and practical HOI data, we utilized HaMeR [23] to elevate the 2D output of the diffusion model to 3D space. Adopting the denoised RGB image as input and given camera intrinsic

parameters, HaMeR can predict the corresponding MANO parameters  $\theta$  and  $\beta$  for the hand, as well as the translation (denoted as  $t$ ) between the camera and hand, thereby the hand components of the 2D HOI can be elevated to 3D.

**Object Reconstruction from Single Image:** Single-image reconstruction [17, 43, 44, 46] is a challenging task that involves generating a complete 3D model from a single image. To achieve this, we employ Michelangelo [46], an advanced generative 3D modeling system capable of producing high-fidelity meshes.

Michelangelo leverages aligned shape-image-text latent representations as conditional inputs for a 3D generative model, which effectively generating detailed 3D shapes with semantic consistency. Utilizing the object image as a conditional input, Michelangelo efficiently generates a congruent 3D mesh model  $\mathcal{M}_{o,r}$ :

$$\mathcal{M}_{o,r} = D(E(I) + \epsilon) \quad (3)$$

where,  $D$  represents the decoder, which reconstructs the 3D shape from the encoded noisy representation.  $E$  represents the encoder, which encodes the input object image  $I$  into a latent noise space, and  $\epsilon$  is the noise. In this paper, the Michelangelo is responsible for reconstructing high-quality 3D mesh models from the object images generated by diffusion.

**Detection-Assisted Scale Alignment:** We independently obtain 3D hand  $\mathcal{M}_h$  and object model  $\mathcal{M}_{o,r}$  from HaMeR and Michelangelo. However, a significant discrepancy exists in the scale ratio between the hand and object when compared to the 2D representations. To address this issue, we perform hand-object detection [29] on the 2D HOI data output from the diffusion model, yielding hand detection boxes  $\mathbf{B}_h$  and object detection boxes  $\mathbf{B}_o$ . Based on this, we further calculate the hand-object scale ratio in the 2D HOI  $k_{2D}$  by computing areas of boxes  $S(\mathbf{B}_h)$  and  $S(\mathbf{B}_o)$ :

$$k_{2D} = \sqrt{\frac{S(\mathbf{B}_h)}{S(\mathbf{B}_o)}} \quad (4)$$

In the 3D space, we calculate the convex hulls  $\mathbf{C}_h$  and  $\mathbf{C}_o$  of the hand and object meshes respectively, and determined the volumes of these convex hulls  $V(\mathbf{C}_h)$  and  $V(\mathbf{C}_o)$  to derive the actual scale ratios  $k_{3D}$  of the reconstructed 3D models:

$$k_{3D} = \sqrt[3]{\frac{V(\mathbf{C}_h)}{V(\mathbf{C}_o)}} \quad (5)$$

By leveraging the scale of hand as a reference, we aligned the scale ratios to derive the scaling factor  $k_{scale}$  for  $\mathcal{M}_{o,r}$ :

$$k_{scale} = \frac{k_{3D}}{k_{2D}} \quad (6)$$

Finally, by scaling the  $\mathcal{M}_{o,r}$  according to this scaling factor, we obtain the object  $\mathcal{M}_o = k_{scale} \cdot \mathcal{M}_{o,r}$  of 3D HOI participants, which is consistent with the hand-object size ratio in the 2D HOI.

### 3.3. Pose Optimization Strategy

**Object Pose Approximation:** Through stage one, we obtain the hand pose parameters  $\theta$ ,  $\beta$  and relative transformation from hand to camera coordinate  $[\mathbf{R}|t]_{h \rightarrow c}$ . However, to achieve a reasonable grasp, we also need the transformation  $[\mathbf{R}|t]_{o \rightarrow c}$  of the object relative to the camera, which we achieve by reprojecting the surface points of object onto the camera plane. Given the intrinsic parameters  $\mathbf{K}$  and the mask image of the object  $M_o$ , we optimize our proposed loss term to get the object to camera transformation. First, we sample  $N$  points  $P_o$  on the object surface using farthest-point sampling. These points are then transformed into the camera coordinate system  $P_{o \rightarrow c}$  using the transformation  $[\mathbf{R}|t]_{o \rightarrow c}$ . We then calculate the point set  $P_{o \rightarrow c}^{2d}$  obtained by projecting the 3D point set of the object onto the 2D plane of the camera:

$$P_{o \rightarrow c}^{2d} = \left\{ [u, v]^T \middle| [u, v, 1]^T = \frac{1}{z(x)} \mathbf{K} \mathbf{x} \middle| \mathbf{x} \in P_{o \rightarrow c} \right\} \quad (7)$$

The z-component of  $\mathbf{x}$  is represented by  $z(\mathbf{x})$ . We fix the camera at  $[0, 0, 0]$  with the view matrix set to the identity matrix  $\mathbf{I}$ . Using the 2D point set  $P_{o \rightarrow c}^{2d}$  derived from the previous calculations, we compute the Chamfer Distance [18] relative to image mask:

$$L_{dist} = \sum_{\mathbf{x} \in P_{o \rightarrow c}^{2d}} \min_{\mathbf{y}} \|\mathbf{x} - \mathbf{y}\|^2 + \sum_{\mathbf{y} \in M_o} \min_{\mathbf{x}} \|\mathbf{x} - \mathbf{y}\|^2 \quad (8)$$

The  $L_{dist}$  ensures that the 2D points projected from the object are aligned as closely as possible to the mask of the segmented object image. Meanwhile, to ensure the correctness of the occlusion between the projected object depth and the hand, we compute the depth regularization  $L_{dep}$  during the projection process:

$$L_{dep} = \sum_{\mathbf{x} \in P_{o \rightarrow c}} I(\mathbf{x}) \cdot \max\{z(\mathbf{x}) - D_r(\mathcal{M}_h, \pi_k(\mathbf{x})), 0\} \quad (9)$$

where  $I(\mathbf{x})$  is an indicator function that determines whether the projection of a given 3D point falls within the mask of the hand.  $\pi_k(\mathbf{x})$  is the projection function, and the  $D_r$  is the rendered depth of the MANO model at the 2D coordinates  $[u, v]$  during optimization. Meanwhile, camera loss  $L_{cam}$  is used to ensure that the object moves in front of the camera and to avoid  $L_{dist}$  and  $L_{dep}$  failing because the object cannot be projected properly if it lies behind the camera. Therefore, the camera loss  $L_{cam}$  is computed as follows:

$$L_{cam} = \frac{1}{|P_{o \rightarrow c}|} \sum_{\mathbf{x} \in P_{o \rightarrow c}} \max\{z(\mathbf{x}), 0\} \quad (10)$$



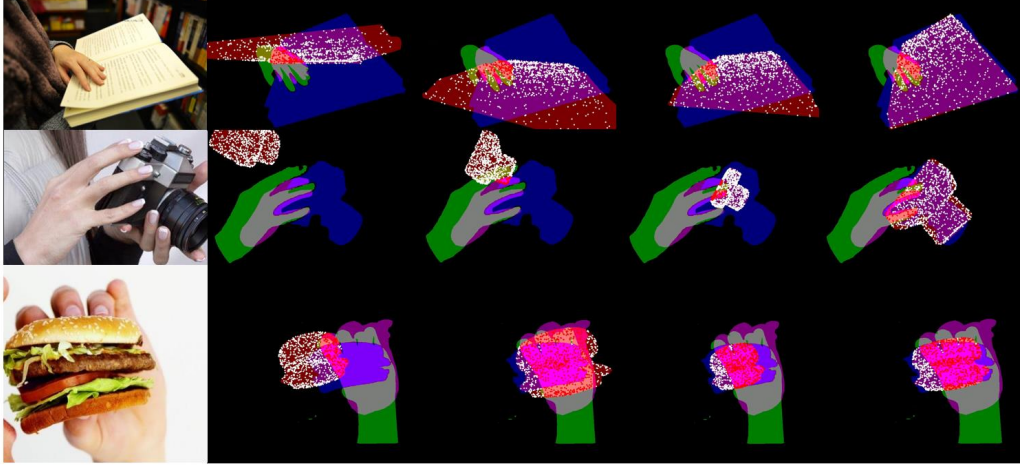


Figure 2. **Object Pose Approximator**: Given the 3D hand-object model generated by FGG, we visualize the optimization process of OPA, using the HOI image generated by diffusion as a guide. The right side shows the process of object pose adjustment.

In summary, our overall optimization loss  $L$  is as follows:

$$L = L_{dist} + \lambda_{dep}L_{dep} + \lambda_{cam}L_{cam} \quad (11)$$

$\lambda_{dep}$  and  $\lambda_{cam}$  are hyperparameters used to adjust awareness degree to different terms.

Fig. 2 illustrates the pose variation of the object after applying the Object Pose Approximator, with the HOI image generated using diffusion serving as the reference image. It demonstrates the evolution of the object pose through the optimization process, showing how the pose gradually aligns with the expected result. The impact of the Chamfer Distance loss is highlighted, as it refines the object positioning to achieve a more accurate and stable grasp.

**Energy Function Guided Contact Optimization:** To further overcome the imperfections existing in the generated HOI scenes—such as floating and interpenetration in the contact between hand and object—we have constructed the following refinement loss function. We first design the  $E_h$  loss term to incorporate the information provided by 2D HOI during the Pose Optimization. Specifically, this term computes the distance between the hand pose at the current optimization step and the estimation results from HaMeR.

Inspired by DexGraspNet [33], we formulate a hand-object pose optimization algorithm, which comprehensively considers common interaction priors to ensure the stability

and naturalness of the grasp. Specifically, our optimization objective is to minimize the following energy function:

$$E_d = w_{dis}E_{dis} + w_{pen}E_{pen} + w_{prior}E_{prior} + w_{spen}E_{spen} \quad (12)$$

Where  $E_{dis}$  is the attraction energy term, calculated as  $E_{dis} = \sum_{i=1}^n d(\mathbf{x}_i, \mathcal{M}_o)$ , ensuring contact between the hand and the object, where  $d(\mathbf{x}_i, \mathcal{M}_o)$  denotes the distance between points on the hand surface and the object mesh, and contact points  $\mathbf{x}_i \in \mathcal{M}_h$  are the points on the hand surface expected to touch the object.  $E_{pen}$  is the repulsion energy term, calculated as  $E_{pen} = \sum_{v \in \mathcal{M}_h} [\mathbf{v} \in \mathcal{M}_o] d(\mathbf{v}, \mathcal{M}_o)$ , which prevents the hand from penetrating the object, where  $[\mathbf{v} \in \mathcal{M}_o]$  is an indicator function that is 1 if point  $\mathbf{v}$  is inside the object mesh and 0 otherwise.  $E_{prior}$  is the prior energy term, used to keep the hand in a natural state, possibly involving regularization of joint angles.  $E_{spen}$  is to penalize self penetration of hand.  $w_{dis}$ ,  $w_{pen}$ ,  $w_{prior}$  and  $w_{spen}$  are weight parameters used to adjust the relative importance of different energy terms in the total energy function. Thus, the overall energy function is given by  $E = \lambda_h E_h + \lambda_d E_d$ . Our configuration of hyperparameters is shown in the supplementary materials.

## 4. Experiments

In this section, we demonstrate the performance of FGS-Net. Section 4.1 details the experimental setup. Section 4.2 discusses the evaluation metrics. In Section 4.3, we compare our method with state-of-the-art approaches. Finally, Section 4.4 validates the effectiveness of the core components through ablation studies.

### 4.1. Implementation Details

All experiments are performed on a system configured with one NVIDIA GeForce RTX 4090 GPU. For the fine-tuning of the diffusion model, we leverage the Adam optimizer with a learning rate set to  $1e-5$  to tune the Stable Diffusion model [25]. This process involves 2000 epochs, drawing inspiration from the DreamBooth [28]. Subsequently, in the pose refinement stage, the Adam [16] optimizer is again engaged to optimize the contact points, maintaining the same learning rate of  $1e-4$  and completing a total of 1000 epochs for this phase.

### 4.2. Metrics and Dataset

**Penetration:** Following [1, 33], we compute two key metrics—Maximal Penetration Depth (MPD) and Solid Intersection Volume (SIV)—to quantitatively measure the degree of penetration between the hand and the object of generated 3D HOI scene.

The MPD is defined as the maximum distance from any penetrated vertex on the hand mesh to the closest point on the surface of the object. MPD effectively captures the deepest point of penetration, accurately identifies the most severe local penetration between the hand and the object. A smaller MPD indicates that the hand is not deeply penetrating the object, which is desirable for generating realistic and physically plausible HOI.

Conversely, the SIV quantifies the total volume of the object that is intersected by the hand mesh, which provides a comprehensive measure of the overall volumetric overlap between the hand and the object. A lower SIV indicates less interpenetration, which is crucial for ensuring the physical plausibility of the hand-object interaction.

**Dataset:** The HO-3D dataset [9] provides 3D pose annotations for scenarios where hands and objects are heavily occluded from each another. It consists of a collection of sequences featuring various individuals interacting with objects selected from the YCB dataset [38]. The HOI4D dataset [20] provides 4D pose annotations for scenarios with complex occlusions between hands and objects during human-object interactions. It includes a series of scenes where different individuals interact with 800 distinct object instances selected from 16 categories in various indoor environments. Additionally, we select functional HOI images from YouTube and other publicly available sources

for training. All images are used to fine-tune the diffusion model, conditioned on their respective functional texts.

### 4.3. Comparison with State-of-the-Art Methods

To evaluate performance of our approach, we compare it with two categories of state-of-the-art methods thereby demonstrate its superiority. Specifically, our experiments consist of two parts: a comparison of 3D reconstruction methods for HOI and a comparison of grasp posture generation methods

To compare with reconstruction approaches, we conduct comparative experiments between our method and single-image HOI 3D reconstruction models, using iHOI [41] as a benchmark. Specifically, we perform experiments on HO-3D [9] and HOI4D [20] datasets, fine-tuning the diffusion model with images from these datasets. For grasp posture generation, we compare our approach with GrabNet [31] and DexGraspNet [33]. For fairness, we use same objects generated from FGG for experiments. All experiments use the official open-source code and provided pre-trained weights to ensure fairness. We design six prompts as inputs to generate corresponding 3D grasping models, aiming to demonstrate performance of our method in 3D hand-object interaction guided by functional text.

Additionally, to visually demonstrate the superiority of our method, we render the 3D HOI results. We first present a comparison on the HO-3D [9] and HOI4D [20] datasets. As illustrated in Fig. 3, the object quality generated by iHOI is poor, and the relative positioning between the hand and the object is also unsatisfactory.

In the comparison with existing grasp generation methods, including GrabNet and DexGraspNet, we visualize the hand grasp postures generated by these methods and our approach. As depicted in Fig. 4, despite GrabNet and DexGraspNet using the 3D models generated in our intermediate process and performing scale alignment, they fail to produce grasp postures that meet functional requirements. When using the diffusion-generated HOI images as a reference image, the grasp postures generated by our method are highly consistent with the reference images, while other methods do not align as well. Additionally, through a quantitative evaluation of grasp quality, as shown in Table. ??, our method outperforms other methods in terms of MPD and SIV metrics, indicating superior grasp quality. As shown in Tab. 1, our method not only meets functional requirements but also does not rely on additional 3D labels, further proving the practicality and efficiency of our approach.

### 4.4. Ablation Study

**Functional Grasp Generator:** In order to verify the effectiveness of our method, we drop the estimated hand gesture parameters and continue using 3D-generated objects

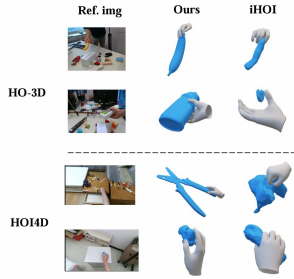


Figure 3. **State-of-the-art comparison:** We compare with iHOI[41] on HO-3D[9] and HOI4D[20]. The images above are with HO-3D images as the reference image, and the ones below are from HOI4D. All images are randomly selected and used for fine-tuning the diffusion model.

	Functional Task	3D Label-free
GrabNet [31]	✗	✗
DexGraspNet [33]	✗	✓
Ours	✓	✓

Table 1. **Capabilities and Limitations of Various Methods:** Comparing to other methods, our FGS-Net complete functional task while keeping 3D label-free.

for subsequent pose optimization. Furthermore, we retain the hand-object alignment process to ensure that the size ratio between the hand and the object remains fitted. As shown in Fig. 5, it is evident that ignoring the hand gesture parameters leads to unpredictable variations in grasping postures, potentially resulting in postures that do not meet the description of input prompt.

**Functional Grasp Refiner:** Functional Grasp Refiner is designed to optimize the hand-object interaction pose to enhance its performance. To validate its effectiveness, we retain the FGG object generating process and conduct separate tests to evaluate the effects of omitting the Object Pose Approximator and energy function optimization. As illustrated in Fig. 5, neglecting Object Pose Approximator results in a significant decline in the performance of hand-object positioning, and the omission of energy function optimization leads to the inability of the hand-object to establish contact. These results underscore the importance of OPA and energy function optimization within our proposed method.

**Core Component:** To validate the effectiveness of our method, we perform ablations on **Object Pose Approximation(OPA)**, **Scale Alignment(SA)**, and the **HaMeR Prior(HP)**. As shown in Fig. 6, eliminating the OPA causes deviations in the 3D hand-object contact position. Scale alignment has a direct impact on model performance due to

the close relationship between object dimensions and subsequent processing steps. Without the HaMeR prior, the 3D grasping position is preserved, but the grasping pose no longer aligns with human intent

## 5. Discussion

Our method is capable of generating corresponding 3D HOI from functional text. However, due to imperfect alignment between the objects generated by the diffusion model and those in the HOI, a bias is introduced during the FGR process. As shown in Fig. 4, the cup generated by FGG is misaligned with the reference image, resulting in inaccuracies such as the thumb not aligning properly with the hand pose in the HOI image when grasping the cup. This emphasizes the critical importance of precise alignment between the object and the HOI to achieve accurate grasping. Misalignment not only causes visual discrepancies but also disrupts the natural interaction between the hand and object, potentially leading to unrealistic or infeasible grasps. To address this issue and enhance grasping accuracy, it is essential to optimize the alignment between the object and the HOI. Misalignment not only impairs visual fidelity but also undermines the practicality and feasibility of the grasp. In future work, we aim to develop a hand removal network to eliminate hand interference, thereby improving alignment accuracy and enabling the generated 3D HOI to more accurately reflect the true position and pose of the object. This will improve the performance and robustness of grasping tasks. By focusing on this aspect, we expect the generated grasps to more effectively represent realistic human-object interactions, further enhancing the model’s applicability in real-world scenarios.

## 6. Conclusion

We propose FGS-Net, a 3D grasp generation framework that uses functional texts to drive the process. FGG generates 3D object models and initial grasp poses, while FGR refines hand-object contact. Our framework ensures both the physical plausibility of contact and functional grasp actions that align with human intent, making the generated grasps task-oriented. A key advantage of FGS-Net is its ability to generate realistic hand-object interaction models without requiring additional 3D annotations. This makes the framework highly scalable and adaptable, suitable for a wide range of real-world grasping tasks. Extensive experimental results demonstrate that FGS-Net significantly enhances grasping quality, accuracy, and usability, proving its superior performance in 3D HOI generation.

## References

- [1] Xiaoyun Chang and Yi Sun. Text2grasp: Grasp synthesis by text prompts of object grasping parts. *arXiv:2404.15189*,

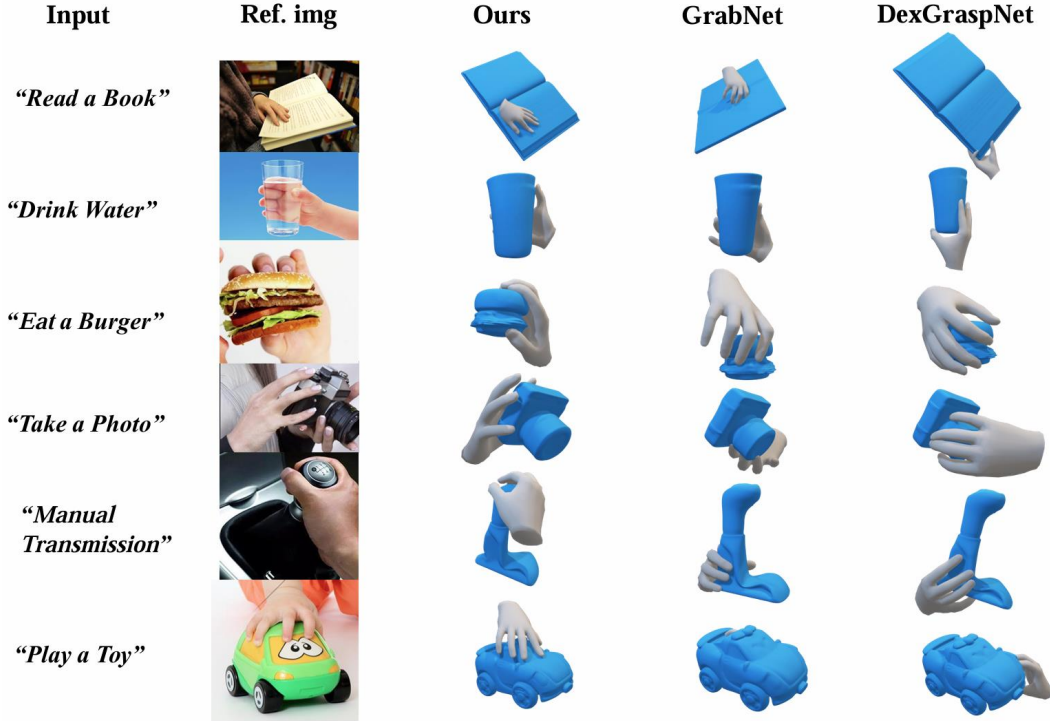


Figure 4. **State-of-the-art comparison:** We compare with GrabNet[31] and DexGrabNet[33]. All images are downloaded from YouTube and other publicly available sources, and are used to fine-tune the diffusion model with the prompts on the left. The images generated by the fine-tuned diffusion model are then used as the basis for subsequent steps.



Figure 5. **Ablation Study of FGG and FGR:** We perform ablation experiment on FGG and FGR separately to demonstrate their effects. FGG refers to keeping only this component, while FGR refers to removing FGG. All experiments use the same prompt.

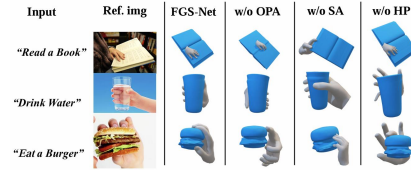


Figure 6. **Ablation Study of Core Component:** We perform ablation on each core component separately to demonstrate their effects, with all experiments using the same prompt.

2024. 1, 2, 6

- [2] Yu-Wei Chao, Wei Yang, Yu Xiang, Pavlo Molchanov, Ankur Handa, Jonathan Tremblay, Yashraj S Narang, Karl Van Wyk, Umar Iqbal, Stan Birchfield, et al. Dexycb: A benchmark for capturing hand grasping of objects. In *CVPR*, pages 9044–9053, 2021. 2
- [3] Jiayi Chen, Yuxing Chen, Jialiang Zhang, and He Wang. Task-oriented dexterous grasp synthesis via differentiable grasp wrench boundary estimator. *arXiv:2309.13586*, 2023.

2

- [4] Zerui Chen, Yana Hasson, Cordelia Schmid, and Ivan Laptev. Alignsdf: Pose-aligned signed distance fields for hand-object reconstruction. In *ECCV*, pages 231–248, 2022. 1, 2
- [5] Zerui Chen, Shizhe Chen, Cordelia Schmid, and Ivan Laptev. gsdf: Geometry-driven signed distance functions for 3d hand-object reconstruction. In *CVPR*, pages 12890–12900, 2023. 1, 2
- [6] Dima Damen, Hazel Doughty, Giovanni Maria Farinella,



- Sanja Fidler, Antonino Furnari, Evangelos Kazakos, Davide Moltisanti, Jonathan Munro, Toby Perrett, Will Price, et al. Scaling egocentric vision: The epic-kitchens dataset. In *ECCV*, pages 720–736, 2018. 1
- [7] Zicong Fan, Maria Pirelli, Maria Eleni Kadoglou, Xu Chen, Muhammed Kocabas, Michael J Black, and Otmar Hilliges. Hold: Category-agnostic 3d reconstruction of interacting hands and objects from video. In *CVPR*, pages 494–504, 2024. 1, 2
- [8] Patrick Grady, Chengcheng Tang, Christopher D Twigg, Minh Vo, Samarth Brahmhatt, and Charles C Kemp. Contactopt: Optimizing contact to improve grasps. In *CVPR*, pages 1471–1481, 2021. 2
- [9] Shreyas Hampali, Mahdi Rad, Markus Oberweger, and Vincent Lepetit. Honnotate: A method for 3d annotation of hand and object poses. In *CVPR*, 2020. 1, 2, 6, 7
- [10] Shreyas Hampali, Sayan Deb Sarkar, Mahdi Rad, and Vincent Lepetit. Keypoint transformer: Solving joint identification in challenging hands and object interactions for accurate 3d pose estimation. In *CVPR*, 2022.
- [11] Yana Hasson, Gül Varol, Dimitris Tzionas, Igor Kalevtykh, Michael J. Black, Ivan Laptev, and Cordelia Schmid. Learning joint reconstruction of hands and manipulated objects. In *CVPR*, 2019. 1, 3
- [12] Yana Hasson, Gül Varol, Cordelia Schmid, and Ivan Laptev. Towards unconstrained joint hand-object reconstruction from rgb videos. In *3DV*, pages 659–668, 2021. 1, 2
- [13] Jonathan Ho, Ajay Jain, and Pieter Abbeel. Denoising diffusion probabilistic models. *Advances in neural information processing systems*, 33:6840–6851, 2020. 3
- [14] Junxing Hu, Hongwen Zhang, Zerui Chen, Mengcheng Li, Yunlong Wang, Yebin Liu, and Zhenan Sun. Learning explicit contact for implicit reconstruction of hand-held objects from monocular images. In *AAAI*, pages 2220–2228, 2024. 1, 2
- [15] Juntao Jian, Xiuping Liu, Manyi Li, Ruizhen Hu, and Jian Liu. Affordpose: A large-scale dataset of hand-object interactions with affordance-driven hand pose. In *ICCV*, pages 14713–14724, 2023. 1
- [16] Diederik P Kingma. Adam: A method for stochastic optimization. *arXiv:1412.6980*, 2014. 6
- [17] Weiyu Li, Jiarui Liu, Rui Chen, Yixun Liang, Xuelin Chen, Ping Tan, and Xiaoxiao Long. Craftsman: High-fidelity mesh generation with 3d native generation and interactive geometry refiner. *arXiv:2405.14979*, 2024. 4
- [18] Shaowei Liu, Saurabh Gupta, and Shenlong Wang. Building rearticulable models for arbitrary 3d objects from 4d point clouds. In *CVPR*, pages 21138–21147, 2023. 4
- [19] Tengyu Liu, Zeyu Liu, Ziyuan Jiao, Yixin Zhu, and Song-Chun Zhu. Synthesizing diverse and physically stable grasps with arbitrary hand structures using differentiable force closure estimator. *ICRA*, 7(1):470–477, 2021. 2
- [20] Yunze Liu, Yun Liu, Che Jiang, Kangbo Lyu, Weikang Wan, Hao Shen, Boqiang Liang, Zhoujie Fu, He Wang, and Li Yi. Hoi4d: A 4d egocentric dataset for category-level human-object interaction. In *CVPR*, pages 21013–21022, 2022. 1, 6, 7
- [21] Toan Nguyen, Minh Nhat Vu, Baoru Huang, Tuan Van Vo, Vy Truong, Ngan Le, Thieu Vo, Bac Le, and Anh Nguyen. Language-conditioned affordance-pose detection in 3d point clouds. In *ICRA*, pages 3071–3078, 2024. 1
- [22] Iason Oikonomidis, Nikolaos Kyriazis, and Antonis A Argyros. Full dof tracking of a hand interacting with an object by modeling occlusions and physical constraints. In *ICCV*, pages 2088–2095, 2011. 2
- [23] Georgios Pavlakos, Dandan Shan, Ilija Radosavovic, Angjoo Kanazawa, David Fouhey, and Jitendra Malik. Reconstructing hands in 3d with transformers. In *CVPR*, pages 9826–9836, 2024. 2, 3, 1
- [24] Alec Radford, Jong Wook Kim, Chris Hallacy, Aditya Ramesh, Gabriel Goh, Sandhini Agarwal, Girish Sastry, Amanda Askell, Pamela Mishkin, Jack Clark, et al. Learning transferable visual models from natural language supervision. In *ICML*, pages 8748–8763, 2021. 3
- [25] Robin Rombach, Andreas Blattmann, Dominik Lorenz, Patrick Esser, and Björn Ommer. High-resolution image synthesis with latent diffusion models. In *CVPR*, pages 10684–10695, 2022. 2, 3, 6
- [26] Javier Romero, Dimitrios Tzionas, and Michael J. Black. Embodied hands: Modeling and capturing hands and bodies together. *SIGGRAPH Asia*, 2017. 2, 3
- [27] Yu Rong, Takaaki Shiratori, and Hanbyul Joo. Frankmocap: A monocular 3d whole-body pose estimation system via regression and integration. In *ICCV Workshops*, 2021. 2
- [28] Nataniel Ruiz, Yuanzhen Li, Varun Jampani, Yael Pritch, Michael Rubinstein, and Kfir Aberman. Dreambooth: Fine tuning text-to-image diffusion models for subject-driven generation. In *CVPR*, pages 22500–22510, 2023. 3, 6, 1
- [29] Dandan Shan, Jiaqi Geng, Michelle Shu, and David F Fouhey. Understanding human hands in contact at internet scale. In *CVPR*, pages 9869–9878, 2020. 4
- [30] Yaoxian Song, Penglei Sun, Piaopiao Jin, Yi Ren, Yu Zheng, Zhixu Li, Xiaowen Chu, Yue Zhang, Tiefeng Li, and Jason Gu. Learning 6-dof fine-grained grasp detection based on part affordance grounding. *arXiv:2301.11564*, 2023. 1
- [31] Omid Taheri, Nima Ghorbani, Michael J Black, and Dimitrios Tzionas. Grab: A dataset of whole-body human grasping of objects. In *ECCV*, pages 581–600, 2020. 6, 7, 8, 2
- [32] Chao Tang, Dehao Huang, Lingxiao Meng, Weiyu Liu, and Hong Zhang. Task-oriented grasp prediction with visual-language inputs. In *IROS*, pages 4881–4888, 2023. 1
- [33] Ruicheng Wang, Jialiang Zhang, Jiayi Chen, Yinzhen Xu, Puhao Li, Tengyu Liu, and He Wang. Dexgraspnet: A large-scale robotic dexterous grasp dataset for general objects based on simulation. In *ICRA*, pages 11359–11366, 2023. 2, 5, 6, 7, 8
- [34] Yangang Wang, Jianyuan Min, Jianjie Zhang, Yebin Liu, Feng Xu, Qionghai Dai, and Jinxiang Chai. Video-based hand manipulation capture through composite motion control. *TOG*, 32(4):1–14, 2013. 2
- [35] Wei Wei, Peng Wang, and Sizhe Wang. Generalized anthropomorphic functional grasping with minimal demonstrations. *arXiv:2303.17808*, 2023. 2

- [36] Yi-Lin Wei, Jian-Jian Jiang, Chengyi Xing, Xian-Tuo Tan, Xiao-Ming Wu, Hao Li, Mark Cutkosky, and Wei-Shi Zheng. Grasp as you say: Language-guided dexterous grasp generation. *arXiv:2405.19291*, 2024. 2
- [37] Zehang Weng, Haofei Lu, Danica Kragic, and Jens Lundell. Dexdiffuser: Generating dexterous grasps with diffusion models. *arXiv:2402.02989*, 2024. 2
- [38] Yu Xiang, Tanner Schmidt, Venkatraman Narayanan, and Dieter Fox. Posecnn: A convolutional neural network for 6d object pose estimation in cluttered scenes. *arXiv:1711.00199*, 2017. 1, 6
- [39] Lixin Yang, Xinyu Zhan, Kailin Li, Wenqiang Xu, Jiefeng Li, and Cewu Lu. Cpf: Learning a contact potential field to model the hand-object interaction. In *ICCV*, pages 11097–11106, 2021. 2
- [40] Lixin Yang, Kailin Li, Xinyu Zhan, Fei Wu, Anran Xu, Liu Liu, and Cewu Lu. Oakink: A large-scale knowledge repository for understanding hand-object interaction. In *CVPR*, pages 20953–20962, 2022. 1
- [41] Yufei Ye, Abhinav Gupta, and Shubham Tulsiani. What’s in your hands? 3d reconstruction of generic objects in hands. In *CVPR*, pages 3895–3905, 2022. 6, 7, 2
- [42] Yufei Ye, Poorvi Hebbbar, Abhinav Gupta, and Shubham Tulsiani. Diffusion-guided reconstruction of everyday hand-object interaction clips. In *ICCV*, pages 19717–19728, 2023. 1, 2
- [43] Biao Zhang, Jiapeng Tang, Matthias Niessner, and Peter Wonka. 3dshape2vecset: A 3d shape representation for neural fields and generative diffusion models. *TOG*, 42(4):1–16, 2023. 4
- [44] Longwen Zhang, Ziyu Wang, Qixuan Zhang, Qiwei Qiu, Anqi Pang, Haoran Jiang, Wei Yang, Lan Xu, and Jingyi Yu. Clay: A controllable large-scale generative model for creating high-quality 3d assets. *TOG*, 43(4):1–20, 2024. 4
- [45] Yibiao Zhang, Jinglue Hang, Tianqiang Zhu, Xiangbo Lin, Rina Wu, Wanli Peng, Dongying Tian, and Yi Sun. Functionalgrasp: Learning functional grasp for robots via semantic hand-object representation. *IEEE Robotics and Automation Letters*, 8(5):3094–3101, 2023. 1
- [46] Zibo Zhao, Wen Liu, Xin Chen, Xianfang Zeng, Rui Wang, Pei Cheng, Bin Fu, Tao Chen, Gang Yu, and Shenghua Gao. Michelangelo: Conditional 3d shape generation based on shape-image-text aligned latent representation. *NeurIPS*, 36, 2024. 4
- [47] Tianqiang Zhu, Rina Wu, Xiangbo Lin, and Yi Sun. Toward human-like grasp: Dexterous grasping via semantic representation of object-hand. In *ICCV*, pages 15741–15751, 2021. 2

# Towards Semantic 3D Hand-Object Interaction Generation via Functional Text Guidance

## Supplementary Material

### A. Details of diffusion model

DreamBooth [28] is a technique for fine-tuning diffusion models that enables users to customize a pre-trained text-to-image model with only a small set of images (typically 3~5) of a specific subject. The main goal is to adapt the model’s output to better align with the given subject, while retaining the ability to generate diverse images. The DreamBooth loss function consists of two main components: **predicted noise residual loss** and **class-specific prior preservation loss**. The combined loss function is defined as:

$$\mathbb{E}_{\mathbf{x}, \mathbf{c}, \epsilon, \epsilon', t} \left[ w_t \|\hat{x}_\theta(\alpha_t \mathbf{x} + \sigma_t \epsilon, \mathbf{c}) - \mathbf{x}\|_2^2 + \lambda w_{t'} \|\hat{x}_\theta(\alpha_{t'} \mathbf{x}_{\text{pr}} + \sigma_{t'} \epsilon', \mathbf{c}) - \mathbf{x}_{\text{pr}}\|_2^2 \right] \quad (13)$$

where,  $\mathbf{x}$  represents the HOI image,  $\mathbf{c}$  is the functional text condition vector,  $\epsilon$  and  $\epsilon'$  are the noise terms, and  $t$  is the time step in the diffusion process. The parameters  $\alpha_t$  and  $\sigma_t$  regulate the noise levels, while  $\alpha_{t'}$  and  $\sigma_{t'}$  serve a similar purpose, and  $\mathbf{x}_{\text{pr}}$  represents a sample generated by the pre-trained diffusion model. The weight factors  $w_t$  and  $w_{t'}$  regulate the contributions of each loss term, and  $\hat{x}_\theta$  represents the diffusion model. The hyperparameter  $\lambda$  adjusts the relative importance of the two loss components.

To fine-tune a pre-trained text-to-image diffusion model, we pair the HOI image  $\mathbf{x}$  with the functional text prompt  $\mathbf{c}$ , as shown in Fig. 10. During training, we set the number of epochs to 2000 and use a learning rate of  $1 \times 10^{-6}$ . In the class-specific prior preservation loss, the hyperparameter  $\lambda$  controls the relative weight of the prior preservation term, which is set to 1. Through DreamBooth fine-tuning, we can obtain the HOI image guided by the functional text prompt.

### B. Details of FGR

In the FGR, we focus on two primary steps: Object Pose Approximation (OPA) and the subsequent Contact Optimization. This section provides a detailed implementation of the FGR algorithm, explaining the key parameters and their configurations involved in this process.

In the OPA stage, using the given object mask  $M_o$ , hand model  $\mathcal{M}_h$ , object model  $\mathcal{M}_o$ , and the relative pose of the hand model  $[\mathbf{R}|\mathbf{t}]_{h \rightarrow c}$ , we roughly estimate the relative pose of the object model  $[\mathbf{R}|\mathbf{t}]_{o \rightarrow c}$ .

We achieve pose estimation by optimizing the three proposed loss groups. For two parameters in  $L_{\text{dep}}$  and  $L_{\text{cam}}$

losses, we set them as  $\lambda_{\text{dep}} = 0.1$  and  $\lambda_{\text{cam}} = 1000$ , respectively, and the optimization step is set to 1000. For the  $[\mathbf{R}|\mathbf{t}]_{o \rightarrow c}$ , we optimize the rotation  $\mathbf{R}_{o \rightarrow c}$  and translation  $\mathbf{t}_{o \rightarrow c}$  with different learning rates separately.

At the beginning of the optimization process, due to the uncertainty in the object’s coordinate system, there is a significant displacement discrepancy. To address this, we increase the learning rate for the relative translation parameters while decreasing the learning rate for the object rotation parameters. As the optimization progresses, we lower the learning rate for the translation parameters and increase the learning rate for the rotation parameters. In our experimental setup, both the translation and rotation learning rates are initialized at  $1 \times 10^{-2}$ . During the iteration process, we use exponential interpolation to gradually adjust the translation learning rate to  $1 \times 10^{-3}$  and the rotation learning rate to  $1 \times 10^{-1}$ . Since large differences in object rotation  $\mathbf{R}_o$  may lead to local minima during pose estimation, we conduct multiple experiments by randomly initializing the object’s rotation. The configuration with the smallest loss is then selected as the final result. The evolution of the OPA-optimized loss curves for the two classes is shown in Fig. 7, which confirms the convergence of OPA, with the optimization video provided in the supplementary materials.

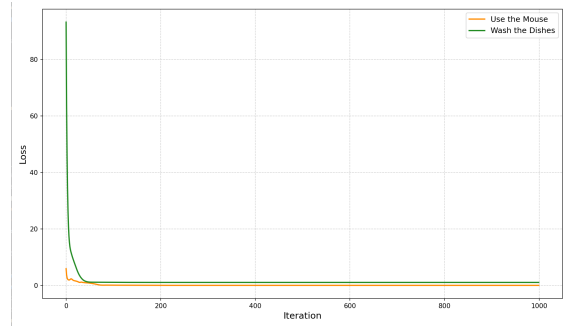


Figure 7. Evolution of the loss curve optimized by OPA.

In the contact optimization stage, we take into account the potential uncertainty in depth information, which in some special cases (such as grasping rod-shaped objects) may lead to intractable local minima. To address this issue, we introduce depth noise and adapt a two-step optimization strategy.

In the first step, we focus on optimizing the depth information of the object, bringing it as close as possible to the hand model provided by HaMeR [23]. During this phase

of optimization, we use  $E_d$  as the error function, with the weight parameters  $w_d = 1$  and  $w_{\text{pen}} = 5$ . The optimization iterations in the first stage are set to 300. In the second step, we make detailed adjustments to the grasping pose of hand.

Through this staged optimization approach, we are able to effectively handle the challenges posed by depth uncertainty and optimize the object pose estimation. To avoid excessive influence of the hand pose on the optimization process (such as when a grasping pose makes it difficult to adjust the object while satisfying the non-penetration condition), we first initialize the hand joint angles. The initial angle is set to  $\theta_{\text{init}} = 0.5 * \theta_{\text{hamer}}$ .

Then, based on the previous stage, we use  $E_d + E_h$ , where the weights in  $E_d$  are set as  $w_{\text{dis}} = 100$ ,  $w_{\text{pen}} = 200$ ,  $w_{\text{prior}} = 0.5$ , and  $w_{\text{spen}} = 10.0$ .  $E_h$  includes  $L_2$  supervision for the pose  $\theta_{\text{hamer}}$  provided by HaMeR and the hand translation  $t_{\text{hamer}}$ , with  $w_{\theta} = 0.5$  and  $w_t = 100$ , and the second-phase optimization is performed for 3000 iterations. In summary, our hyperparameter settings are shown in the Tab. 2.

Table 2. Hyperparameters for Object Pose Approximation (OPA) and Contact Optimization.

Stage	Parameter	Value
<b>OPA</b>	$\lambda_{\text{cam}}$	1000
	$\lambda_{\text{dep}}$	0.1
	step	1000
	$\text{LR}_{\text{t\_init}}$	$1 \times 10^{-2}$
	$\text{LR}_{\text{t\_final}}$	$1 \times 10^{-3}$
	$\text{LR}_{\text{R\_init}}$	$1 \times 10^{-2}$
<b>Contact Optimization</b>	$\text{LR}_{\text{R\_final}}$	$1 \times 10^{-1}$
	step one	300
	$w_d$	1
	$w_{\text{pen}}$	5
	step two	3000
	$w_{\text{dis}}$	100
	$w_{\text{pen}}$	200
	$w_{\text{prior}}$	0.5
	$w_{\text{spen}}$	10.0
	$\theta_{\text{init}}$	$0.5 * \theta_{\text{hamer}}$
	$w_{\theta}$	0.5
	$w_t$	100

Table 3. Comparison of Contact Ratios. Our method significantly reduces interpenetration with only a slight decrease in contact area.

	Ours	GrabNet [31]	DexGraspNet [33]
CR(%)	13.3	14.5	17.1

## C. Additional Experiments

We conduct a comparative experiment with the latest HOI reconstruction algorithm, HOLD[7], on the HO-3D [9] dataset. In the experiment, we utilize the pretrained model and official open-source code provided by HOLD. As shown in the Fig. 8, HOLD exhibits poor performance in object reconstruction, which negatively impacts the overall visual quality. Moreover, HOLD heavily relies on high-quality video data and requires extended training time. In contrast, our algorithm can generate high-quality HOI 3D models solely based on input text, significantly improving efficiency and applicability.



Figure 8. We compare with iHOI[41] and HOLD[7] on HO-3D[9].

Reducing interpenetration metrics at the expense of physical plausibility can lead to increased distances between the hand and the object, thereby degrading the quality of generated 3D hand-object interactions. Our method significantly reduces interpenetration while maintaining physical plausibility, synthesizing high-quality hand-object interaction scenes. We demonstrate this through the contact area between the hand and the object. Specifically, we consider vertices where the distance between the hand and the object is less than 0.01 meters as **contact vertices**, and we visualize the faces containing these vertices as contact surfaces. As shown in the Fig. 9, due to tolerance of interpenetration, DexGraspNet[33] and GrabNet[31] achieve larger contact areas. In contrast, our method generates more natural hand-object contact without noticeable interpenetration phenomena. We define the **Contact Ratio (CR)** as the proportion of contact vertices to the total number of object vertices. Quantitative results presented in Tab. 3 demonstrate numerically that our method results in only a slight decrease in contact area. Meanwhile, the Fig. 11 shows the 3D HOI generation results under 15 different text prompts, with all corresponding 3D models (.obj files) included in the supplementary materials.



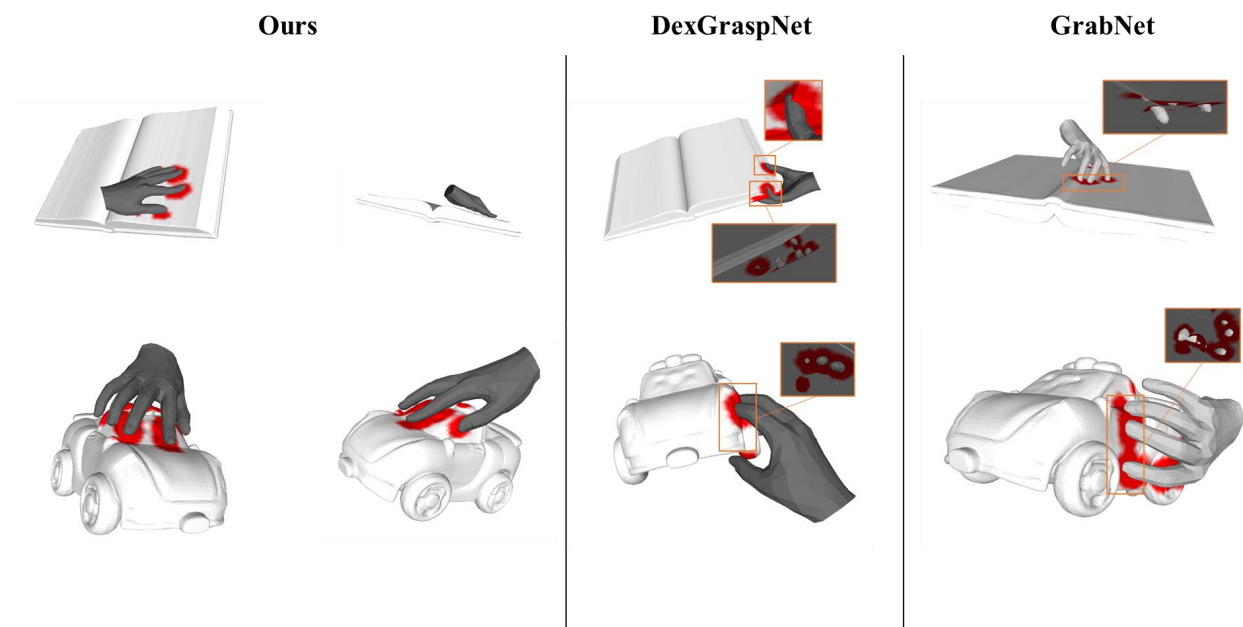


Figure 9. Contact Area (red) and Interpenetration.



Figure 10. The image-text pairs used for fine-tuning the Diffusion model.

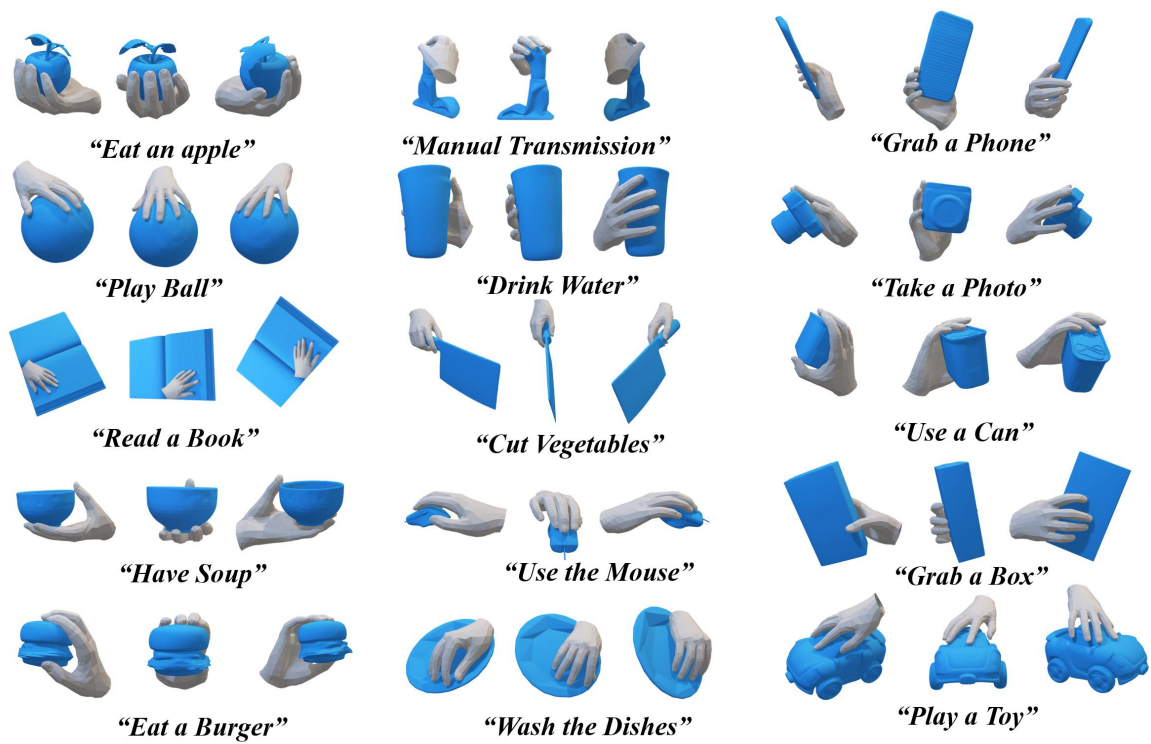


Figure 11. Visualization of generated 3D HOI scenes when using functional text inputs.